Research Article

Omer A. Alawi*, Haslinda Mohamed Kamar*, Mayadah W. Falah, Omar A. Hussein, Ali H. Abdelrazek, Waqar Ahmed, Mahmoud Eltaweel, Raad Z. Homod, Nadhir Al-Ansari, and Zaher Mundher Yaseen

Thermohydraulic performance of thermal system integrated with twisted turbulator inserts using ternary hybrid nanofluids

https://doi.org/10.1515/ntrev-2022-0504
received August 22, 2022; accepted January 2, 2023

Abstract: Mono, hybrid, and ternary nanofluids were tested inside the plain and twisted-tape pipes using k-omega shear stress transport turbulence models. The Reynolds number was 5,000 ≤ Re ≤ 15,000, and thermophysical properties were calculated under the condition of 303 K. Single nanofluids (Al_2O_3/distilled water [DW], SiO_2/DW, and ZnO/DW), hybrid nanofluids (SiO_2 + Al_2O_3/DW, SiO_2 + ZnO/DW, and ZnO + Al_2O_3/DW) in the mixture ratio of 80:20, and ternary nanofluids (SiO_2 + Al_2O_3 + ZnO/DW) in the mixture ratio of 60:20:20 were estimated in different volumetric concentrations (1, 2, 3, and 4%). The twisted pipe had a higher outlet temperature than the plain pipe, while SiO_2/DW had a lower T_{out} value with 310.933 K (plain pipe) and 313.842 K (twisted pipe) at Re = 9,000. The thermal system gained better energy using ZnO/DW with 6178.060 W (plain pipe) and 8426.474 W (twisted pipe). Furthermore, using SiO_2/DW at Re = 9,000, heat transfer improved by 18.017% (plain pipe) and 21.007% (twisted pipe). At Re = 900, the pressure in plain and twisted pipes employing SiO_2/DW reduced by 167.114 and 166.994%, respectively. In general, the thermohydraulic performance of DW and nanofluids was superior to one. Meanwhile, with Re = 15,000, DW had a higher value of $\eta_{\text{Thermohydraulic}} = 1.678$.

Keywords: heat transfer properties, hydrodynamic performance, ternary hybrid nanofluid, twisted-tape pipes, energy turbulators

* **Corresponding author: Omer A. Alawi,** Department of Thermofluids, School of Mechanical Engineering, Universiti Teknologi Malaysia, 81310 UTM Skudai, Johor Bahru, Malaysia, e-mail: omeralawi@utm.my
* **Corresponding author: Haslinda Mohamed Kamar,** Department of Thermofluids, School of Mechanical Engineering, Universiti Teknologi Malaysia, 81310 UTM Skudai, Johor Bahru, Malaysia, e-mail: haslinda@utm.my
Mayadah W. Falah: Building and Construction Techniques Engineering Department, Al-Mustaqbal University College, Hillah 51001, Iraq, e-mail: mayadahwaheed@mustaqbal-college.edu.iq
Omar A. Hussein: Petroleum System Control Engineering Department, College of Petroleum Processes Engineering, Tikrit University, Tikrit, Iraq, e-mail: omar_assi2008@yahoo.com
Ali H. Abdelrazek: Department of Mechanical Precision Engineering, Takasago i-Kohza, Malaysia-Japan International Institute of Technology, Universiti Teknologi Malaysia, Kuala Lumpur, Malaysia, e-mail: ali.h.razek@outlook.com
Waqar Ahmed: Greater Bay Area Institute of Precision Medicine, Guangzhou 511462, China, e-mail: Waqarum.ah@gmail.com
Mahmoud Eltaweel: School of Physics, Engineering and Computer Science, University of Hertfordshire, Hatfield, AL10 9AB, United Kingdom, e-mail: m.eltaweel@herts.ac.uk
Raad Z. Homod: Department of Oil and Gas Engineering, Basrah University for Oil and Gas, Basrah, Iraq, e-mail: raadahmood@yahoo.com
Nadhir Al-Ansari: Department of Civil, Environmental and Natural Resources Engineering, Lulea University of Technology, 97187, Lulea, Sweden, e-mail: nadhir.alansari@ltu.se
Zaher Mundher Yaseen: Civil and Environmental Engineering Department, King Fahd University of Petroleum and Minerals, Dhahran 31261, Saudi Arabia, e-mail: zaheryaseen88@gmail.com

Nomenclature

Ag	silver
Al_2O_3	aluminum oxide
CMC	containing carboxymethyl cellulose
CoTs	co-twisted tapes
C_p	specific heat capacity (J/kg K)
CTs	counter-twisted tapes
Cu	copper
CuO	copper oxide
D_h	hydraulic diameter (m)
DW	distilled water
f	friction factor

Fe	iron
FOM	figure of merit
k	thermal conductivity (W/m K)
L	pipe's total length (m)
$\dot{m}$	mass flow rate (kg/s)
MgO	magnesium oxide
MWCNTs	multi-walled carbon nanotubes
nf	nanofluids
np	nanoparticles
Nu_{avg}	average Nusselt number
PCM	phase change material
PEC	performance assessment criteria
P_{out}	pressure outlet (Pa)
PP	plain pipe
Pt	platinum
Re	Reynolds number
SiO_2	silicon dioxide
SST	shear stress transport
SWCNTs	single-walled carbon nanotubes
T_{in}	inlet fluid temperature (K)
TiO_2	titanium dioxide
T_{out}	outlet fluid temperature (K)
TP	twisted pipe
TPF	thermal performance factor
T_w	wall temperature (K)
ZnO	zinc oxide
α	twist ratio
β	width/depth
η	enhancement Index
ρ	density (kg/m^3)
Φ	mass fraction of nanoparticles
μ	dynamic viscosity (Ns/m^2)

1 Introduction

1.1 Study background and motivation

Pipes are the thermal system to exchange (dissipate) the heat from different engineering, industrial, and manufacturing applications. Tremendous energy is extensively consumed using heat exchangers in power plants, heating, and cooling systems, leading to global warming. New heat-exchanging systems with better thermal efficiency are needed in this matter [1,2]. Heat can be transported by three mechanisms: active, passive, and compound [3]. The active method uses external energy sources like mechanical support, resulting in a more complex/heavy system and higher production costs [4]. Meanwhile, the passive method utilizes the internal energy of the system to enhance heat transport efficiency by changing the flow pattern of the circulating medium or selecting high thermal conductivity fluids [5]. The combination of twisted-tape inserts and nanofluid is the technical solution within a heat exchanger [6]. Despite the significant advantages of applying the passive approach, such as higher heat transfer performance, low cost, and less maintenance, it still shows higher pressure loss [7,8]. As a result, the compound approach incorporates active and passive procedures into a single system.

1.2 Adopted literature review on nanofluid-based twisted pipes

Laboratory work and numerical simulations were performed using the passive methodology to evaluate the thermal efficiency of twisted-tape tubular heat exchangers [9]. Khoshvaght-Alabadi *et al.* [10] tested experimentally three twist ratios (α = 0.33, 0.67, and 1) with different values of width/depth for peripheral cuts (β = 0.33, 0.5, 0.67, 1, 1.5, 2, and 3) and three metallic nanofluids (Cu/distilled water [DW], Fe/DW, and Ag/DW). A maximum enhancement of 18.2% was identified using Ag/DW compared with base fluid, while the maximum rise in the pressure drop is only 8.5%. Also, 25 and 39 mm pitch wire coil turbulators were examined experimentally in heat transfer and pressure loss in the presence of Al_2O_3/DW in different concentrations [11]. The increase in heat transfer was larger when a 25 mm pitch wire coil was used in the fluid than when a 39 mm pitch wire coil was used. Meanwhile, the friction factor of the heat exchanger with turbulators was greater than that of the heat exchanger without turbulators. Furthermore, TiO_2/DW nanofluid was tested in twisted-tape inserts in a dimpled pipe [12]. The maximum thermo-hydraulic performance of 1.258 was attained by inserting twisted tape with a twist ratio of 3 and 0.15vol%-TiO_2/DW in a dimple angle of 45°. The heat transfer and CuO/DW nanofluid flow were simulated through a helical profiled pipe under turbulent single-phase and two-phase scenarios [13]. The most excellent performance efficiency coefficient in a tube with one twisted tape was 2.18, but it was 2.04 in a tube with two twisted tapes under the conditions of two-phase flow, Re = 36,000 and 4vol%-CuO/DW. The turbulent flow and heat transfer of a non-Newtonian aqueous solution containing carboxymethyl cellulose (CMC) and CuO nanoparticles in plain and helical profiled tubes were numerically investigated [14]. The averaged total thermal performance criterion using a twist ratio of 5 and 1.5% nanofluids was 2.02, with an

enhancement of 38% relative to that at a twist ratio of 83 and 0.1% nanofluids. The effects of twisted-tape inserts on heat transfer parameters and pressure drop using graphene oxide nanofluid were computationally discussed and optimized through an artificial neural network and genetic algorithm [15]. Based on the results, the optimal inputs are Re = 19,471, the twist pitch is 0.0376, and the volume fraction is 0.0383, producing Nu of 263.57 and a friction factor of 0.0725.

Meanwhile, investigators need much attention to evaluate nanocomposites inside pipes with twisted-tape turbulators. The hydrothermal properties (Nu_{avg} = 132%) and (f = 55%) increased by reducing the twist ratio, reducing the V-cut width ratio, and increasing the V-cut depth ratio in the presence of Al_2O_3@TiO_2/DW [16]. Maddah *et al.* [17] concluded that applying Al_2O_3@TiO_2 hybrid nanofluid inside a double pipe heat exchanger modified with twisted-tape insertion increased the exergy efficiency. A higher V-cut depth or lower width ratio yielded more heat transfer and pressure drop in the presence of DW-based Al_2O_3 and phase change material (PCM) nanofluids and Al_2O_3 + PCM hybrid nanofluids [18]. Bahiraei *et al.* [19] analyzed the entropy generation of graphene–platinum (Gr@Pt) hybrid nanofluid in double co-twisted tapes (CoTs) and double counter-twisted tapes (CTs) with various twisted ratios. The CoTs were recommended based on the outcomes since they demonstrated a reduced entropy production rate. Also, experimental reports on Al_2O_3@MgO hybrid nanofluid utilizing a tapered wire coil turbulator were investigated by Singh and Sarkar [20]. They observed that the maximum value of thermal performance factor (TPF) was 1.69 for D-type wire coil. The heat transfer properties, pressure loss, and hydrothermal efficiency were experimentally examined using various V-cut twisted-tape and tapered wire coil configurations in the presence of Al_2O_3@MWCNT hybrid nanofluid [9]. For all arrangements, the performance assessment criteria (PEC) and figure of merit (FOM) were found to be >1. The V-cut twisted tape with a twist ratio of 5, a depth ratio of 0.5, and a width ratio of 0.5 represented the maximum values of PEC and FOM, whereas the least values were found in C- and D-type tapered wire coil. The thermal performance of MoS_2–Ag/DW hybrid nanofluid was tested inside a solar collector having wavy strips in the absorber tube [21]. The results revealed that using composite nanofluid with a 5% concentration in a twisted strip with a height of 40 mm provided the highest heat transfer rate. Moreover, the energy (η_{th}), exergy (η_{ex}), and PEC of DW-based MWCNT-MgO hybrid nanofluid were discussed inside a parabolic solar collector having a symmetrical twisted turbulator [22]. Their two-phase mixed model showed that the values of PEC are more than 1 for all cases. In addition, for case of φ = 3%, as Re increased from 10,000 to 25,000, η_{th} and η_{ex} were enhanced by 45.98 and 31.67% for pitch ratio (PR) = 1 and 0.25, respectively. In another numerical study, the maximum value of PEC is 4.7 and belongs to Re = 12,000 for a pipe with a lower number of turns (case 2), where Φ = 1% [23]. They utilized $((CH_2OH)_2)$/Cu–SWCNT hybrid nanofluid with different volume concentrations and Reynolds numbers. In this regard, the simulation of ternary hybrid nanofluids is carried out by suspending six different nanoparticle combinations and four different surface profiles of regenerative evaporative coolers [24]. Compared with the flat surface, the maximum energy performance, coefficient of performance, and exergy efficiency were 30, 10.68, and 0.29%, respectively. Moreover, the performances of different water-based binary hybrid nanofluids (Al_2O_3–Cu, Al_2O_3–CNTs, Al_2O_3–graphene, Cu–graphene, and Cu–CNTs, CNTs + graphene) and tri-hybrid nanofluids (Al_2O_3–Cu–CNTs–water, Al_2O_3–Cu–graphene, Al_2O_3–CNTs–graphene, Cu–CNTs–graphene–water) at 100 W and 0.9vol% were tested for single-phase natural circulation loop [25]. It can be observed that the ternary nanofluid shows better performance than the binary nanofluids [26,27]. The ternary nanofluids have a lower reduction in mass flow rate, higher enhancement in effectiveness, and higher reduction in the entropy generation rate as compared to water [28].

1.3 Research novelty and objectives

According to the previous studies and works of researchers, it can be easily recognized that less attention was paid to the problems of twisted tapes using ternary hybrid nanofluids. Accordingly, one of the motivations of the current research is to examine a new type of twisted tape based on ternary hybrid nanofluids. In the current research, single nanofluids (Al_2O_3/DW, SiO_2/DW, and ZnO/DW), hybrid nanofluids (SiO_2 + Al_2O_3/DW, SiO_2 + ZnO/DW, and ZnO + Al_2O_3/DW) in the mixture ratio of 80:20, and ternary nanofluids (SiO_2 + Al_2O_3 + ZnO/DW) in the mixture ratio of 60:20:20 were compared with different volumetric concentrations (1, 2, 3, and 4%). The shear stress transport (SST k-ω) three-dimensional turbulence model was used to solve the thermohydraulic performance. The favorable properties (heat transfer) and negative properties (frictional pressure drop) were optimized to select the practical working fluids in engineering systems. The previous experimental and numerical investigations on nanofluids as working fluids in twisted pipes are summarized in Table 1.

Table 1: Previous experimental and numerical investigations on the use of nanofluids as working fluids in twisted pipes

Ref.	Nanofluids	Type of study	Specifications	Remarks
[10]	Cu/DW, Fe/DW, and Ag/DW	Experimental	U-tube heat exchanger using spiky TT	Maximum η at $\alpha = \beta = 0.33$
[13]	CuO–DW	Computational	One–two TT	PEC = 2.18 (1-TT) and PEC = 2.04 (2-TT)
[14]	CMC@CuO–DW	Computational	TT with H/D = 5, 10, 15, and 83	PEC = 2.02, using 1.5vol% and H/D = 5
[15]	Graphene oxide–DW	Computational	TT with P/W = 7.03, 3.51, and 2.34	Maximum PEC value at P/W = 2.34
[16]	Al_2O_3@TiO_2–DW	Experimental	TT with different H/D, V-cut depth ratios, and V-cut width ratios	TPF >1 for hybrid nanofluid for all modified twisted-tape inserts
[18]	Al_2O_3@PCM–DW	Experimental	TT with different H/D, V-cut depth ratios, and V-cut width ratios	A higher V-cut depth or lower width ratio yields more heat transfer and pressure drop
[19]	GNPs@Pt–DW	Computational	TT with CoTs and CTs	CTs reduced total entropy generation rate more than CoTs
[21]	MoS_2@Ag–DW	Computational	Simple, wavy, and twisted tapes	Wavy and twisted tapes had the lowest and highest PEC
[22]	MWCNT–MgO–DW	Computational	PSC integrated with TTs with various pitch ratios	As Re increased from 10,000 to 25,000, η_{th} and η_{ex} were enhanced by 45.98 and 31.67% for PR = 1 and 0.25, respectively
[23]	EG–Cu–SWCNTs	Computational	PTC integrated with helical axial fines	The maximum PEC value was 4.7 and belonged to Re = 12,000 for a pipe with a lower number of turns (case 2), in which φ = 1%
Current study	Al_2O_3/DW, SiO_2/DW, and ZnO/DW; SiO_2 + Al_2O_3/DW and SiO_2 + ZnO/DW; and ZnO + Al_2O_3/DW, and SiO_2 + Al_2O_3 + ZnO/DW	Computational	Tilted TT with 45°	DW showed higher $\eta_{Thermohydraulic}$ values than nanofluids

2 Numerical methodology

2.1 Physical model and numerical method

The basic configuration under examination is a plain pipe with $L = 900$ mm and $D_h = 20$ mm. Meanwhile, the twisted pipe has the same total length and hydraulic diameter. The helical profile length, width, and path were 20 mm, 0.5 mm, and 30 mm, respectively. Meanwhile, the twisted-tape angle was 45°. Different heat transfer fluids such as DW, single nanofluids, hybrid nanofluids, and ternary nanofluids enter the heat exchangers under the conditions of $T_{in} = 303$ K, different volumetric concentrations, and different Reynolds numbers. The external walls of plain and twisted-tape pipes were heated under a constant heat flux to study the heat transfer enhancement parameters.

The schematic diagram of the twisted-tape insert pipe is illustrated in Figure 1, along with the applied boundary conditions and the grid domain. Here, the input variables are the inlet temperature T_{in}; the wall temperature T_w; the inlet velocity v_{in}; the outlet pressure P_{out}, which is set to atmospheric pressure; and the different geometrical parameters. As for the output parameters, P_{in} is set to be the pressure at the inlet, which is compared against P_{out}, the pressure at the end of the twisted pipe, which is the relevant section of the simulation. Temperature T_{out} is also taken at the end of the twisted pipe. The twisted tape does not cover the full length of the pipe because pressure outlets near obstacles can produce backflow errors, leading to poor convergence [29].

The pressure-based solver has been applied in this simulation. Meanwhile, the partial differential equations have been solved (discretized) by the second-order upwind method using ANSYS FLUENT 2020R1 software based on the finite volume method. All computational fluid dynamics simulations in this study are run with double-precision variables to avoid such inaccuracies. Iteration errors occur when solutions are not completely converged or oscillate between values. This error is frequently addressed by performing enough iterations to ensure convergence. Furthermore, the SIMPLE (Semi-Implicit Method for Pressure-Linked Equations) Consistent algorithm is implemented to couple the velocity and pressure. It should be noted that the convergence for the residual of mass and momentum and energy equations is considered below 10^{-3} and 10^{-6}, respectively.

2.2 Mathematical formulations and assumptions

The nanofluids employed to improve heat transport are typically diluted solid–liquid blends. These metallic particles can roughly be said to act like a fluid because they are fluidizable and ultrafine (less than 100 nm). The nanofluid can be considered a regular pure fluid if it is assumed that there is no motion slip between the discontinuous phase of the scattered ultrafine particles and the continuous liquid and that there is local thermal equilibrium between the nanoparticles and the fluid [30,31]. In this study, the effective single-phase flow works due to the above assumptions and hypotheses.

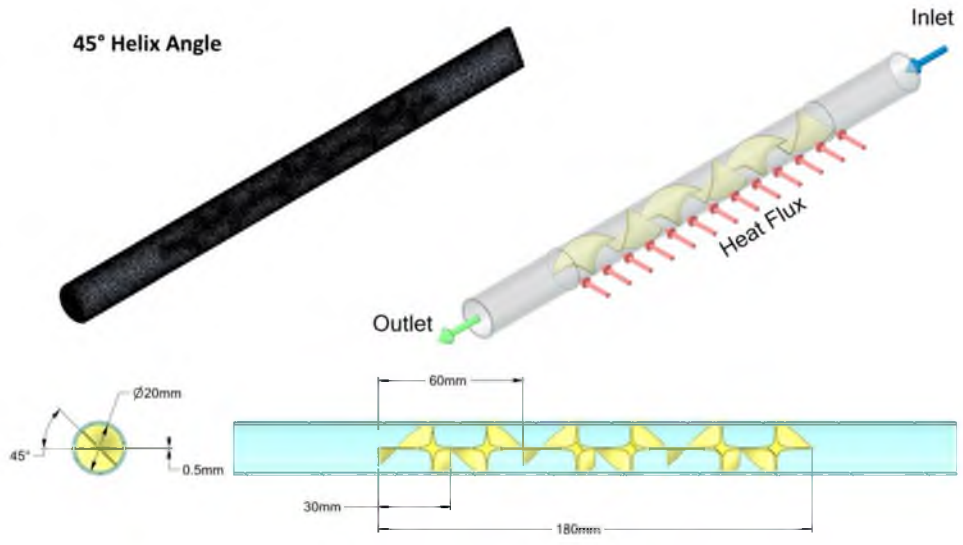

Figure 1: Physical problem and computational domain of pipe with twisted-tape inserts.

The nanofluid flow is assumed to be turbulent, incompressible, Newtonian, and steady-state conditions. In this study, compression work and viscous heating are not significant. The thicknesses of the inner and outer pipe walls are not considered. All the equations of continuity, motion, and energy for the pure fluid are directly extended to the nanofluid [32]:

Governing equation for mass:

$$\nabla\cdot(\rho\vec{V}) = 0, \tag{1}$$

Governing equation for momentum:

$$\nabla\cdot(\rho\vec{V}\vec{V}) = -\nabla P + \nabla\cdot((u + u_t)(\nabla\vec{V} + \nabla\vec{V}^T)) + \rho\vec{g}, \tag{2}$$

Governing equation for energy transport:

$$\nabla\cdot(\rho C_p\vec{V}) = \nabla\cdot(k_{\text{eff}}\nabla T) + \rho\epsilon, \tag{3}$$

where $\vec{V}$ is the mean velocity vector, $K_{\text{eff}} = K + K_t$ is the effective thermal conductivity of covalent and non-covalent nanofluids, and ϵ is the energy dissipation rate.

The turbulent nanofluid flow in plain and twisted pipes was simulated in this work for Reynolds numbers ranging from 5,000 to 15,000. These simulations and the convective heat transfer coefficient were calculated using Menter's two-equation SST k-ω turbulence model, which uses the benefits of the k-ω model and the k-ε model by defining weight functions [33,34]. Governing equations of the SST k-ω turbulence model are as follows:

Kinematic eddy viscosity:

$$\nu_T = \frac{a_1 k}{\max(a_1\omega, SF_2)}, \tag{4}$$

Turbulence kinetic energy:

$$\frac{\partial k}{\partial t} + U_j\frac{\partial k}{\partial x_j} = P_k - \beta^* k\omega + \frac{\partial}{\partial x_j}\left((\nu + \sigma_k\nu_T)\frac{\partial k}{\partial x_j}\right), \tag{5}$$

Specific dissipation rate:

$$\frac{\partial \omega}{\partial t} + U_j\frac{\partial \omega}{\partial x_j} = \alpha S^2 - \beta\omega^2 + \frac{\partial}{\partial x_j}\left((\nu + \sigma_\omega\nu_T)\frac{\partial \omega}{\partial x_j}\right) + 2(1 - F_1)\sigma_{\omega^2}\frac{1}{\omega}\frac{\partial k}{\partial x_i}\frac{\partial \omega}{\partial x_i}, \tag{6}$$

Closure coefficients and auxiliary relations:

$$F_2 = \tanh\left(\max\left(\frac{2\sqrt{k}}{\beta^*\omega y}, \frac{500\nu}{y^2\omega}\right)^2\right), \tag{7}$$

$$P_k = \min\left(\tau_{ij}\frac{\partial U_i}{\partial x_j}, 10\beta^* k\omega\right), \tag{8}$$

$$F_1 = \tanh\left(\left(\min\left(\max\left(\frac{2\sqrt{k}}{\beta^*\omega y}, \frac{500\nu}{y^2\omega}\right), \frac{4\sigma_{\omega^2}k}{CD_{k\omega}y^2}\right)\right)^4\right), \tag{9}$$

$$CD_{k\omega} = \max\left(2\rho\sigma_{\omega^2}\frac{1}{\omega}\frac{\partial k}{\partial x_i}\frac{\partial \omega}{\partial x_i}, 10^{-10}\right), \tag{10}$$

$$\phi = \phi_1 F_1 + \phi_2(1 - F_1), \tag{11}$$

$$\alpha_1 = \frac{5}{9}, \alpha_2 = 0.44,$$

$$\beta_1 = \frac{3}{40}, \beta_2 = 0.0828,$$

$$\beta^* = \frac{9}{100},$$

$$\sigma_{k_1} = 0.85, \sigma_{k_2} = 1,$$

$$\sigma_{\omega_1} = 0.5, \quad \sigma_{\omega_2} = 0.856, \tag{12}$$

where S is the strain rate magnitude and y is the distance to the next surface. Meanwhile, α_1, α_2, β_1, β_2, β^*, σ_{k_1}, σ_{k_2}, σ_{ω_1}, and σ_{ω_2} represent all model constants. F_1 and F_2 refer to the blending functions. Note that $F_1 = 1$ inside the boundary layer and 0 in the free stream.

The turbulent convective heat transfer and nanofluid flow are examined through several parameters as follows [35]:

Reynolds number:

$$\text{Re} = \frac{\rho\nu D_h}{\mu}, \tag{13}$$

Prandtl number:

$$\text{Pr} = \frac{\mu C_p}{k}, \tag{14}$$

Heat gain (W):

$$Q_{\text{Gain}} = \dot{m} \times C_p \times (T_{\text{out}} - T_{\text{in}}), \tag{15}$$

Heat transfer coefficient (W/m^2. K):

$$h_{tc} = \frac{Q_{\text{Gain}}}{A \times (\overline{T}_w - \overline{T}_f)}, \tag{16}$$

Nusselt number:

$$Nu_{\text{avg}} = \frac{hD_h}{k}, \tag{17}$$

Friction factor:

$$f = \frac{2 \times \Delta P \times D_h}{\rho \times \nu^2 \times L}, \tag{18}$$

Pressure drop:

$$\Delta P = P_{\text{in}} - P_{\text{out}}, \tag{19}$$

Dittus–Boelter equation:

$$Nu_{avg} = 0.023 \times Re^{0.8} \times Pr^{0.4}, \quad (20)$$

Blasius equation:

$$f = \frac{0.3164}{Re^{0.25}}, \quad (21)$$

Thermohydraulic performance:

$$\eta_{Thermohydraulic} = \frac{Nu_{TP}}{Nu_{PP}} \Big/ \left(\frac{f_{TP}}{f_{PP}}\right)^{1/3}, \quad (22)$$

where ρ, v, D_h, and μ refer to the density, working fluid velocity, hydraulic diameter, and dynamic viscosity. C_p and k are the specific heat capacity and thermal conductivity of the working fluid. Also, $\dot{m}$ refers to the mass flow rate and $T_{out} - T_{in}$ represents the outlet/inlet difference temperatures. TP and PP refer to twisted and plain pipes. $A = \pi DL$, $\bar{T}_f = \frac{(T_{out} - T_{in})}{2}$, and $\bar{T}_w = \sum \frac{T_w}{n}$.

3 Thermophysical properties of mono, hybrid, and ternary nanofluids

The thermophysical properties of single, hybrid, and ternary nanofluids were estimated empirically through a set of equations and models under 303 K. Nanofluids are preferred because nanoparticles have a larger surface-to-volume ratio than bulk materials [36], resulting in unique behavior. The suspension of nanoparticles into base fluids augments the thermophysical properties of heat transfer fluids [37]. In the literature, several studies have discussed the thermophysical properties of single and double nanofluids [38–40]. The development of innovative triple nanofluids has recently gained considerable interest [41,42]. In this research, three different nanomaterials, such as Al_2O_3, SiO_2, and ZnO, were suspended in DW in different volumetric concentrations (1, 2, 3, and 4%) (Table 2). The hybrid nanofluids were SiO_2@Al_2O_3/DW, SiO_2@ZnO/DW, and ZnO@Al_2O_3/DW in the mixture ratio of 80:20. Meanwhile, the ternary nanofluids were SiO_2@Al_2O_3 + ZnO/DW in the mixture ratio of 60:20:20. The current mixing ratios are optimized using Prandtl number values. As a result, the selected mixing cases have a higher Prandtl number than base fluids, resulting in improved heat transfer mechanisms. The density of single, hybrid, and ternary nanofluids can be predicted *via* the following set of equations [41]:

Table 2: Thermophysical properties of base fluids and nanomaterials at 303 K [44]

	DW	Al_2O_3	SiO_2	ZnO
Density, ρ (kg/m³)	995.65	3,970	2,200	5,600
Specific heat, C_p (J/kg K)	4178.8	765	703	495.2
Thermal conductivity, k (W/m K)	0.6182	40	1.2	13
Dynamic viscosity, μ (Ns/m²)	7.97×10^{-04}	/	/	/

$$\rho_{nf} = \Phi_{np}\rho_{np} + (1 - \Phi_{np})\rho_{DW}, \quad (23a)$$

$$\rho_{nf} = \Phi_{np_1}\rho_{np_1} + \Phi_{np_2}\rho_{np_2} + (1 - \Phi_{np_1} - \Phi_{np_2})\rho_{DW}, \quad (23b)$$

$$\rho_{nf} = \Phi_{np_1}\rho_{np_1} + \Phi_{np_2}\rho_{np_2} + \Phi_{np_3}\rho_{np_3} + (1 - \Phi_{np_1} - \Phi_{np_2} - \Phi_{np_3})\rho_{DW}. \quad (23c)$$

Moreover, the specific heat capacity of single, hybrid, and ternary nanofluids can be predicted *via* the following set of equations [41]:

$$C_{p_{nf}} = \Phi_{np}\rho_{np}C_{p_{np}} + (1 - \Phi_{np})\rho_{DW}C_{p_{DW}}/\rho_{nf}, \quad (24a)$$

$$C_{p_{nf}} = \Phi_{np_1}\rho_{np_1}C_{p_{np_1}} + \Phi_{np_2}\rho_{np_2}C_{p_{np_2}} + (1 - \Phi_{np_1} - \Phi_{np_2})\rho_{DW}C_{p_{DW}}/\rho_{nf}, \quad (24b)$$

$$C_{p_{nf}} = \Phi_{np_1}\rho_{np_1}C_{p_{np_1}} + \Phi_{np_2}\rho_{np_2}C_{p_{np_2}} + \Phi_{np_3}\rho_{np_3}C_{p_{np_3}} + (1 - \Phi_{np_1} - \Phi_{np_2} - \Phi_{np_3})\rho_{DW}C_{p_{DW}}/\rho_{nf}. \quad (24c)$$

As a result, the following equations may be used to estimate the thermal conductivity of single, hybrid, and ternary nanofluids [43]:

$$\frac{k_{nf_1}}{k_{DW}} = \frac{k_{np_1} + 2k_{DW} + 2\Phi(k_{np_1} - k_{DW})}{k_{np_1} + 2k_{DW} - \Phi(k_{np_1} - k_{DW})}, \quad (25a)$$

$$\frac{k_{nf_2}}{k_{DW}} = \frac{k_{np_2} + 2k_{DW} + 2\Phi(k_{np_2} - k_{DW})}{k_{np_2} + 2k_{DW} - \Phi(k_{np_2} - k_{DW})}, \quad (25b)$$

$$\frac{k_{nf_3}}{k_{DW}} = \frac{k_{np_3} + 2k_{DW} + 2\Phi(k_{np_3} - k_{DW})}{k_{np_3} + 2k_{DW} - \Phi(k_{np_3} - k_{DW})}, \quad (25c)$$

$$k_{nf} = \frac{(k_{nf_1}\Phi_1 + k_{nf_2}\Phi_2 + k_{nf_3}\Phi_3)}{\Phi}. \quad (25d)$$

Similarly, the dynamic viscosity of single, hybrid, and ternary nanofluids may also be calculated using the equations as follows [43]:

$$\mu_{nf_1} = \mu_{DW}(1 + 2.5\Phi_1 + \Phi_1^2), \quad (26a)$$

$$\mu_{nf_2} = \mu_{DW}(1 + 2.5\Phi_2 + \Phi_2^2), \quad (26b)$$

$$\mu_{nf_3} = \mu_{DW}(1 + 2.5\Phi_3 + \Phi_3^2), \quad (26c)$$

$$\mu_{nf} = \frac{(\mu_{nf_1}\Phi_1 + \mu_{nf_2}\Phi_2 + \mu_{nf_3}\Phi_3)}{\Phi}. \quad (26d)$$

4 Results and discussion

4.1 Verification and validation with literature

Grid independence tests were carried out for three grid sizes to ensure that the simulations were independent of the grid size. Numerical instability caused by the mesh, or the model can occasionally impair the convergence. Discretization errors happen when the mesh is not precise or of appropriate quality, frequently representing the geometry incorrectly or failing to reflect the gradients present in the problem adequately. Four different grids were plotted against the Nusselt number (Nu_{avg}) from the Dittus–Boelter equation (Figure 2a) and friction factor (f) from the Blasius equation (Figure 2b). Grids 1, 2, 3, and 4 were with a number of elements of 374,609, 228,925, 194,025, and 152,742. The average errors among grids 1, 2, 3, and 4 with Dittus–Boelter and Blasius equations were 4.233 and 2.102%, 3.244 and 4.773%, 3.124 and 5.843%, and 2.947 and 6.683%, respectively. The accuracy of Nu_{avg} readings increased by decreasing the number of elements. Meanwhile, the accuracy of friction factor values showed completely different behaviors. Grid 2 was used to assess thermohydraulic performance as the main mesh domain in the simulation cases.

The study of Eiamsa-ard *et al.* [45] was used as the validation reference. They experimentally discussed the heat transfer rate (Nu_{avg}), friction factor (f), and thermal enhancement index (η) of DW flow in a tube fitted with twin twisted tapes. Their results demonstrated that the Nusselt number (Nu_{avg}), friction factor (f), and thermal enhancement index (η) increase with decreasing twist ratio. In Figure 3(a and b), the experimental values of Nu_{avg} and f were compared with the current numerical results. The average errors between the experimental and numerical results were 4.406% (Nu_{avg}) and 10.497% (f), respectively.

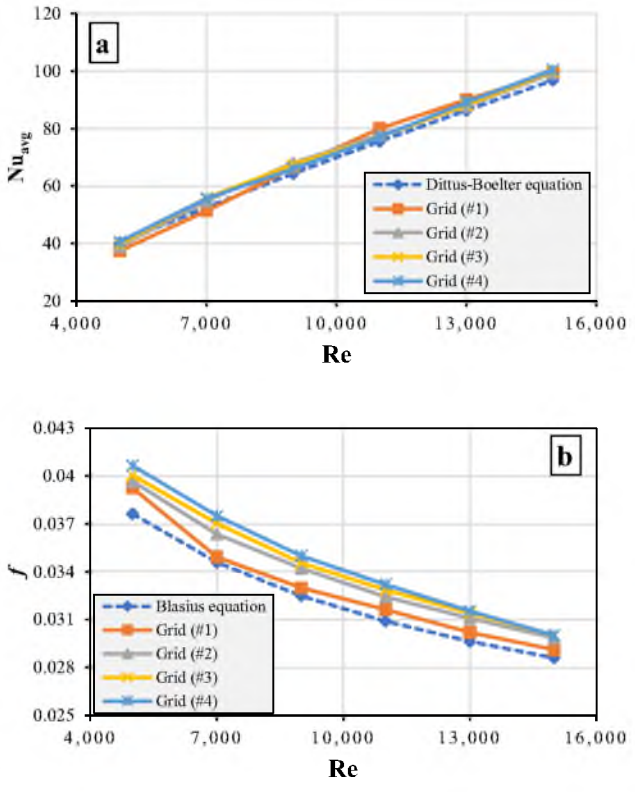

Figure 2: Grid independence results between simulation and empirical correlations for DW: (a) average Nusselt number and (b) friction factor.

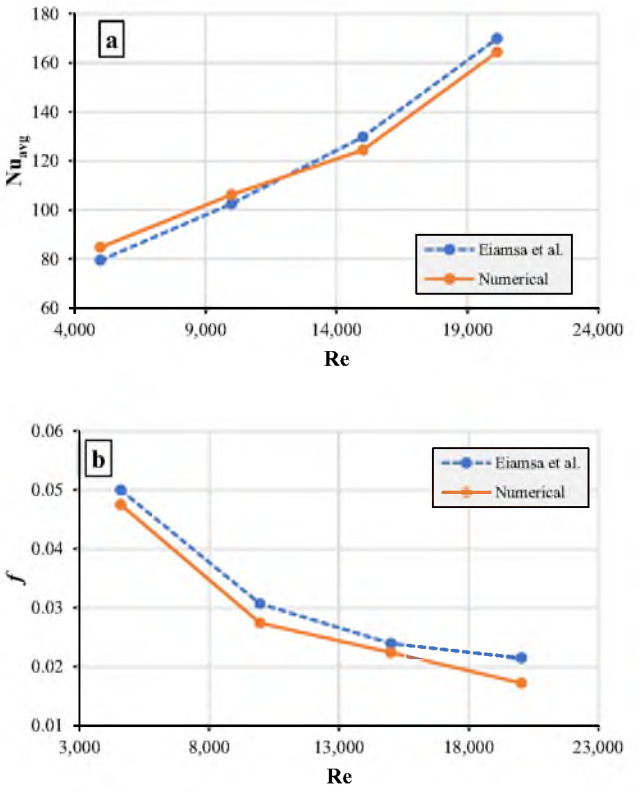

Figure 3: Comparison between the experimental [45] and numerical results: (a) average Nusselt number and (b) friction factor for DW.

4.2 Thermophysical properties

The number of nanoparticles added to the base fluids significantly impacts the thermophysical properties of nanofluids. The thermophysical properties of single nanofluids (Al_2O_3/DW, SiO_2/DW, and ZnO/DW), hybrid nanofluids (SiO_2@Al_2O_3/DW, SiO_2@ZnO/DW, and ZnO@Al_2O_3/DW) in the mixing ratio of 80:20, and ternary nanofluids (SiO_2@Al_2O_3-ZnO/DW) in the mixture ratio of 60:20:20 were estimated using equations and correlations under the condition of 303 K. As shown in Table 3, density, thermal conductivity, and viscosity were increased by increasing the volumetric concentration. Meanwhile, the specific heat was decreased by increasing the volumetric concentration. ZnO/DW achieved the highest density enhancement with 18.554% and ZnO+Al_2O_3/DW with 16.946% at 4vol%. The highest drop in the specific heat was 14.514% by ZnO/DW, and the ternary nanofluid showed a slight decrement by about 1.518% at 4vol%. Also, the best improvement in thermal conductivity was presented by Al_2O_3/DW, ZnO/DW, and ZnO+Al_2O_3/DW by about 20.600, 17.785, and 14.830%, respectively, at 4vol%. The augmentation in the thermal conductivity of single, double, and triple nanofluids can be attributed to the nature of heat transport in nanoparticles and clustering phenomena, the Brownian motion of nanoparticles, and liquid layering at the particle interface [46]. Moreover, hybrid and ternary nanofluids reduced the undesired increment in the dynamic viscosity from 67.383 to 40.668 and 24.086%, respectively, at 4vol%. Meanwhile, the growth in dynamic viscosity of ternary nanofluids relative to DW can be credited to the other layer mixture in the triple nanofluid. As nanoparticle volume fraction increases, dynamic viscosity of nanofluids increases. Also, the increase in the viscosity of the triple nanofluid is attributed to the internal viscous stress and the formation of clusters in the fluid [47,48].

4.3 Thermohydraulic enhancement of plain pipe

In this section, single, hybrid, and ternary nanofluids with 4vol% are tested in the plain pipe under different Reynolds numbers through various parameters, including outlet temperature, heat gain, heat transfer coefficient, average Nusselt number, friction factor, and pressure loss. The outlet temperature of the base fluid and nanofluids decreases by increasing the working fluid velocity inside the plain pipe (Figure 4a). The higher outlet temperature was presented by base fluid (DW); meanwhile, SiO_2/DW nanofluids show a lower T_{out} value. This behavior is due to a change in nanofluid properties (*i.e.*, density and dynamic viscosity) by increasing the Reynolds number at the constant volumetric fraction. The thermal system gains more heat by increasing the Reynolds number for base fluid and all types of nanofluids (single, hybrid, and ternary) (Figure 4b). ZnO/DW and Al_2O_3/DW nanofluids show the best energy gain. Meanwhile, base fluid and SiO_2+Al_2O_3+ZnO/DW offer the worst heat gain performance. Figure 4c and d exhibits the heat transfer enhancement parameters (h_{tc} and Nu_{avg}) for base fluid and nanofluids at different Reynolds numbers. h_{tc} and Nu_{avg} enhance by increasing Reynolds number for DW, single, hybrid, and ternary nanofluids. Al_2O_3/DW nanofluid shows a higher heat transfer coefficient. Meanwhile, SiO_2/DW nanofluid presents higher values of Nu_{avg}. The heat transfer is enhanced by using higher nanoparticle volumetric fraction and nanofluids with better thermal conductivity. The condition of constant Reynolds number for base fluid and nanofluids leads to an increase in dynamic velocity and density values. Therefore, the lower temperature gradients enhance the heat transfer efficiency [35]. Figure 4(e and f) illustrates the pressure drop and friction factor values of DW, single, hybrid, and ternary nanofluids in 4vol% at different Reynolds numbers. The pressure loss increases as the Reynolds number increases, but the friction factor decreases. As shown in Figure 4e, DW presents the lower pressure loss against Re, and single nanofluids show higher pressure reduction values in the order of SiO_2/DW, Al_2O_3/DW, and ZnO/DW, respectively. Because the friction factor is only determined by the Reynolds number, using different working fluids (DW and nanofluids) has no effect.

4.4 Thermohydraulic enhancement of twisted pipe

In this section, single, hybrid, and ternary nanofluids with 4vol% are tested in the twisted pipe under different Reynolds numbers through various parameters, including outlet temperature, heat gain, heat transfer coefficient, average Nusselt number, friction factor, and pressure loss. The outlet temperature of the water and nanofluids decreases by increasing the working fluid velocity inside the plain pipe (Figure 5a), which can be attributed to short heat exchange duration. The higher outlet temperature was presented by base fluid (DW); meanwhile,

Table 3: Thermophysical properties of DW and different types of single, hybrid, and triple nanofluids at 303 K

Properties	Al_2O_3/DW				SiO_2/DW				ZnO/DW			
	1%	2%	3%	4%	1%	2%	3%	4%	1%	2%	3%	4%
ρ (kg/m³)	1021.694	1047.737	1073.781	1099.824	1007.694	1019.737	1031.781	1043.824	1041.694	1087.737	1133.781	1179.824
C_p (J/kg K)	4058.513	3944.205	3835.443	3731.831	4103.833	4030.637	3959.150	3889.312	3980.775	3799.514	3632.976	3479.436
k (W/m K)	0.6949	0.7109	0.7286	0.7470	0.6412	0.6421	0.6457	0.6501	0.6817	0.6966	0.7127	0.7296
μ (Ns/m²)	8.79×10^{-04}	9.84×10^{-04}	1.12×10^{-03}	1.30×10^{-03}	8.79×10^{-04}	9.84×10^{-04}	1.12×10^{-03}	1.30×10^{-03}	8.79×10^{-04}	9.84×10^{-04}	1.12×10^{-03}	1.30×10^{-03}
	$SiO_2 + Al_2O_3$/DW [80:20]				SiO_2 + ZnO/DW [80:20]				ZnO + Al_2O_3/DW [80:20]			
	1%	2%	3%	4%	1%	2%	3%	4%	1%	2%	3%	4%
ρ (kg/m³)	1010.494	1025.337	1040.181	1055.024	1014.494	1033.337	1052.181	1071.024	1037.694	1079.737	1121.781	1163.824
C_p (J/kg K)	4094.669	4012.973	3933.609	3856.478	4078.562	3981.979	3888.856	3799.009	3996.083	3827.595	3671.737	3527.139
k (W/m K)	0.6509	0.6505	0.6526	0.6556	0.6483	0.6479	0.6500	0.6530	0.6807	0.6899	0.7003	0.7113
μ (Ns/m²)	8.51×10^{-04}	9.16×10^{-04}	9.96×10^{-04}	1.09×10^{-03}	8.51×10^{-04}	9.16×10^{-04}	9.96×10^{-04}	1.09×10^{-03}	8.51×10^{-04}	9.16×10^{-04}	9.96×10^{-04}	1.09×10^{-03}
	$SiO_2 + Al_2O_3$ + ZnO/DW [60:20:20]				$SiO_2 + Al_2O_3$ + ZnO/DW [50:30:20]				$SiO_2 + Al_2O_3$ + ZnO/DW [60:20:20]			
	1%	2%	3%	4%	1%	2%	3%	4%	1%	2%	3%	4%
ρ (kg/m³)	1017.294	1038.937	1060.581	1082.224	1017.294	1038.937	1060.581	1082.224	1017.294	1038.937	1060.581	1082.224
C_p (J/kg K)	4069.528	4049.162	4028.796	4008.430	4069.528	4049.162	4028.796	4008.430	4069.528	4049.162	4028.796	4008.430
k (W/m K)	0.6583	0.6570	0.6582	0.6603	0.6583	0.6570	0.6582	0.6603	0.6583	0.6570	0.6582	0.6603
μ (Ns/m²)	8.31×10^{-04}	8.70×10^{-04}	9.14×10^{-04}	9.65×10^{-04}	8.31×10^{-04}	8.70×10^{-04}	9.14×10^{-04}	9.65×10^{-04}	8.31×10^{-04}	8.70×10^{-04}	9.14×10^{-04}	9.65×10^{-04}

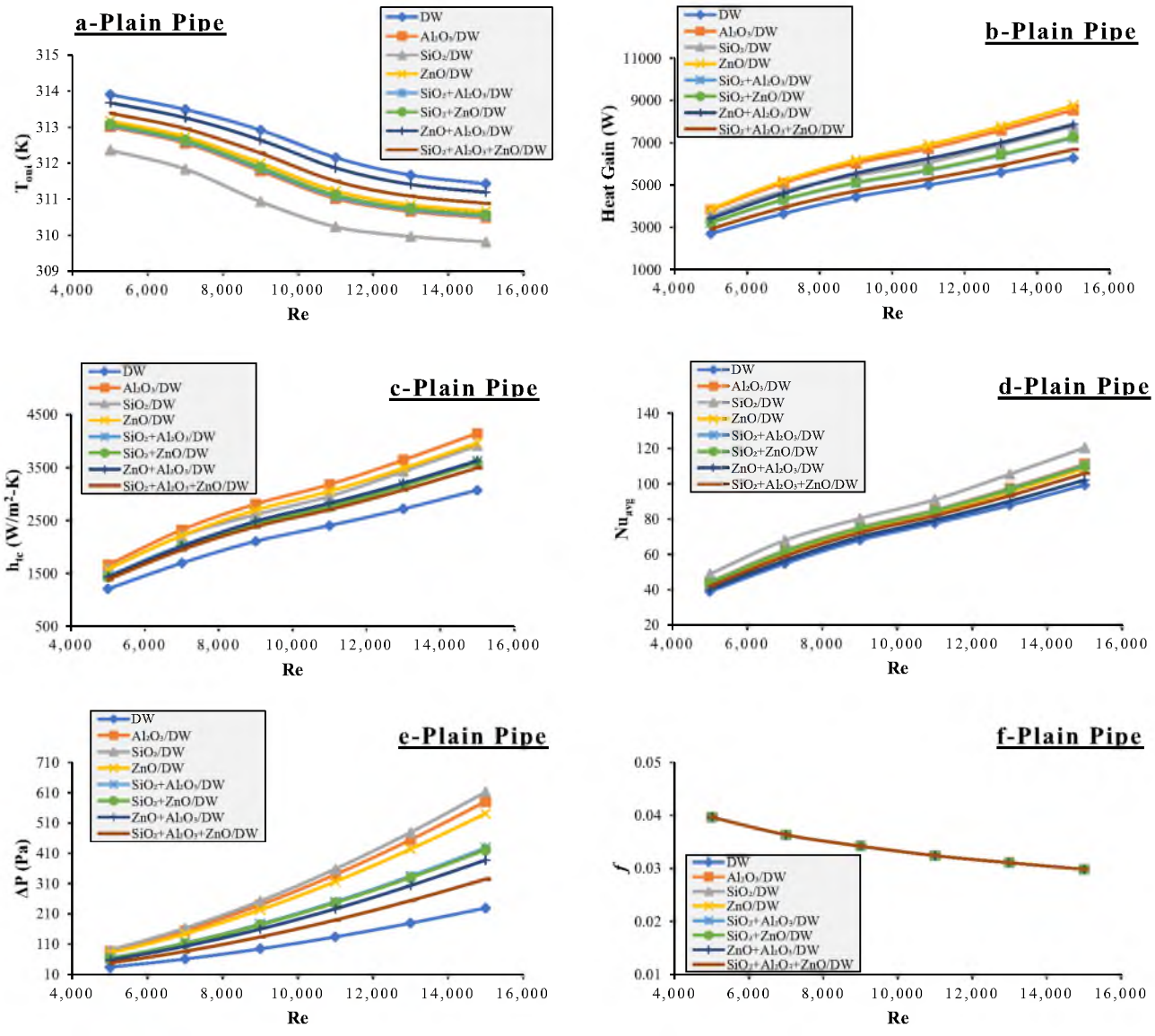

Figure 4: Thermohydraulic parameters of plain pipe using DW, single, hybrid, and ternary nanofluids: (a) outlet temperature, (b) heat gain, (c) heat transfer coefficient, (d) average Nusselt number, (e) pressure loss, and (f) friction factor.

SiO_2/DW nanofluid shows a lower value of T_{out}. The thermal system gains more heat by increasing Reynolds numbers for base liquid and all types of nanofluids (single, hybrid, and ternary) (Figure 5b). ZnO/DW and Al_2O_3/DW nanofluids show the best energy gain. Meanwhile, water and SiO_2 + Al_2O_3 + ZnO/DW show the worst heat gain performance. According to equation (15), and because the inlet temperature for DW and nanofluids has been fixed, three primary parameters are playing a major role in the system absorbing more heat and energy, which are mass flow rate, C_p, and working fluid outlet temperature. Figure 5c and d exhibits the heat transfer enhancement parameters (h_{tc} and Nu_{avg}) for base fluid and nanofluids at different Reynolds numbers. h_{tc} and Nu_{avg} enhance by increasing Reynolds number for DW, single, hybrid, and ternary nanofluids. Al_2O_3/DW nanofluid shows a higher heat transfer coefficient. Meanwhile, SiO_2/DW nanofluid presents higher values of Nu_{avg}. The use of twisted-tape turbulator has significantly influenced flow directions in heated pipes. The helical shape twisted-tape turbulator may induce swirl fluid flow in pipes and promote fluid mixing along the walls. Turbulators can be used to destroy turbulent fluid layers in twisted pipes, improving heat transfer performance [49,50]. However, this phenomenon might result in a larger pressure drop penalty in twisted pipes with nanofluids. The values of pressure drop and friction factor of DW, single, hybrid, and ternary nanofluids in 4vol% at various Reynolds

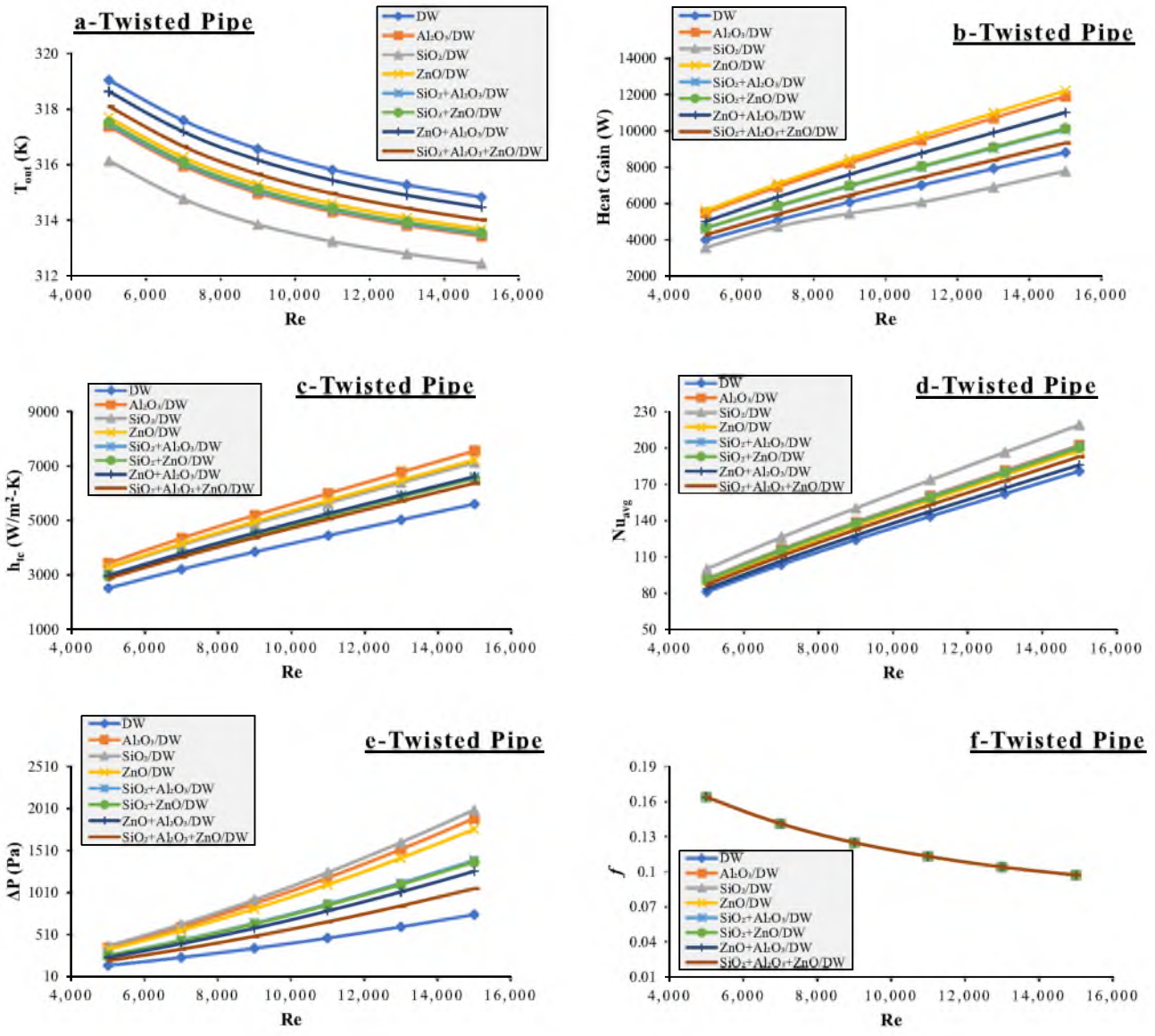

Figure 5: Thermohydraulic parameters of twisted pipe using DW, single, hybrid, and ternary nanofluids: (a) outlet temperature, (b) heat gain, (c) heat transfer coefficient, (d) average Nusselt number, (e) pressure loss, and (f) friction factor.

numbers are shown in Figure 5(e and f). The pressure loss increases as the Reynolds number increases, but the friction factor decreases. As shown in Figure 5e, DW has a more minor pressure loss than Re, but single nanofluids have larger pressure reduction values in the order of SiO_2/DW, Al_2O_3/DW, and ZnO/DW. Employing various working fluids, such as DW and different types of nanofluids, has little impact because the friction factor is solely dictated by the Reynolds number (Figure 5f). Furthermore, inserting twisted tape causes more significant pressure decreases. The increase in pressure drop with increasing Reynolds number is because of the rise in nanofluid viscosity, which produces more friction loss and a greater, more significant pressure drop [35].

4.5 Comparison of plain and twisted pipes

Figure 6 discusses the enhancements/improvements in the thermohydraulic parameters using plain and twisted pipes under 4vol% and Re = 900. In general, T_{out} increases in the twisted pipe by about 1.056% relative to the plain pipe using the same working fluids. In both plain and twisted pipes, SiO_2/DW presents the lower increment in the outlet temperature, followed by Al_2O_3/DW, SiO_2 + Al_2O_3/DW, SiO_2 + ZnO/DW, ZnO/DW, SiO_2 + Al_2O_3 + ZnO/DW, and ZnO + Al_2O_3/DW. This can be attributed to the formation of rotational flow throughout the tube, good flow mixing, and subsequently better heat transfer in the twisted-tape tube. Also, heat gain increases in the twisted

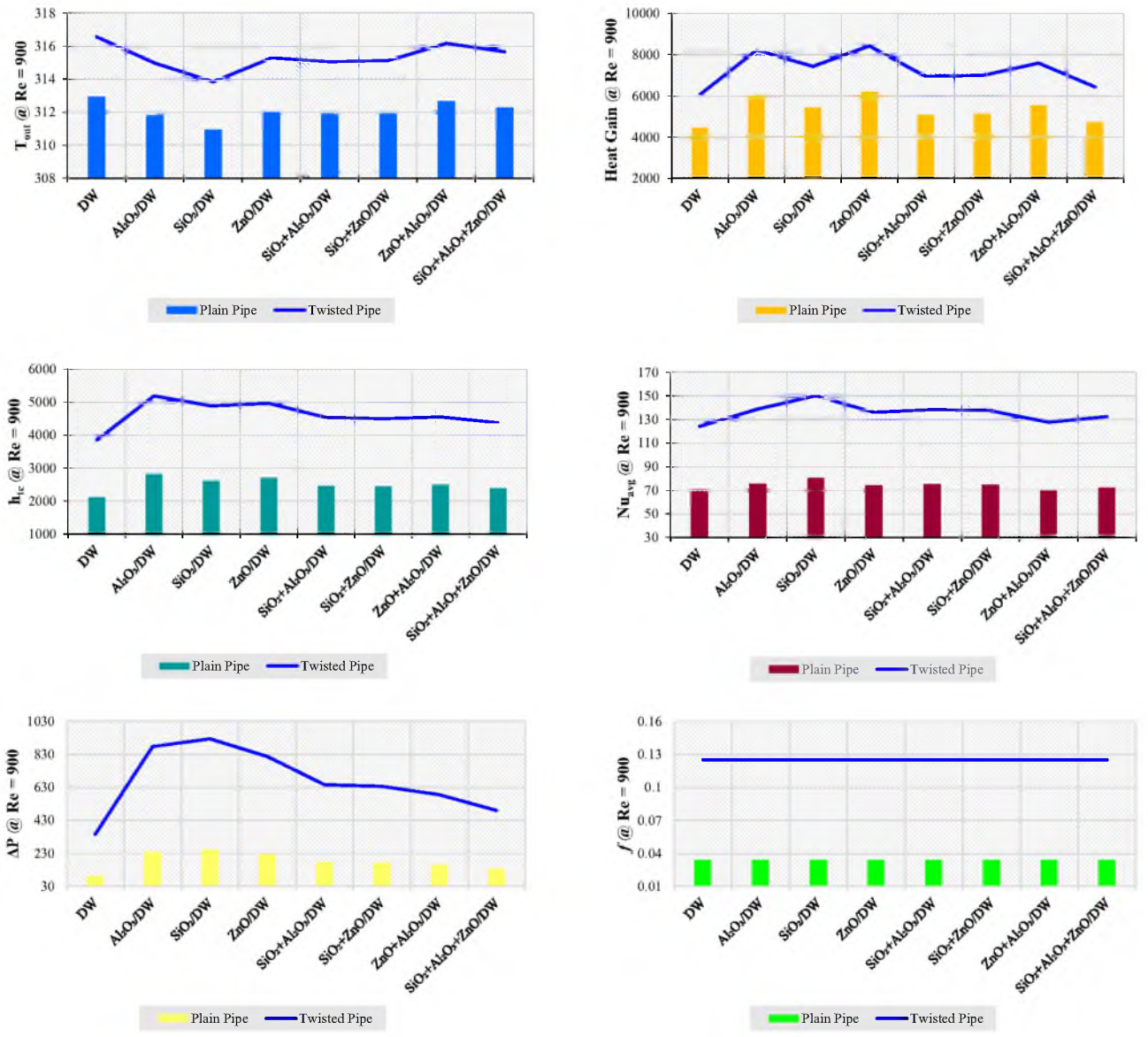

Figure 6: Thermohydraulic parameters of plain and twisted pipes using DW, single, hybrid, and ternary nanofluids at Re = 900 and 4vol%.

pipe by about 36.469% relative to the plain pipe using the same working fluids. ZnO/DW presents the best enhancements in the heat gain values with 39.259% (plain pipe relative to DW) and 38.914% (twisted pipe relative to DW) followed by Al_2O_3/DW with 35.841% (plain pipe relative to DW) and 35.406% (twisted pipe relative to DW). Moreover, hybrid (ZnO + Al_2O_3/DW) nanofluid shows 25.360% (plain pipe relative to DW) and 25.186% (twisted pipe relative to DW). Heat transfer parameters (h_{tc} and Nu_{avg}) enhance the twisted pipe by about 84.009% relative to the plain pipe using the same working fluids (DW and different nanofluids). Al_2O_3/DW presents best enhancements in the heat transfer parameter values with 33.427% (plain pipe relative to DW) and 34.928% (twisted pipe relative to DW). Meanwhile, lowest enhancements in the heat transfer parameters values are presented by SiO_2 + Al_2O_3 + ZnO/DW with 13.122% (plain pipe relative to DW) and 13.720% (twisted pipe relative to DW). Heat transfer parameters improved as the Reynolds number increased due to the rising turbulence level in the twisted pipe and a higher mixing of the working fluid. Inserting twisted tapes inside the pipe significantly improved heat transfer (relative to plain pipe). The fluid moving through the small gaps has a more incredible velocity, resulting in a thinning of the thermal/velocity boundary layer and, consequently, an increase in heat transfer [50]. Moreover, the heat transfer depends on the changes in thermal conductivity

values using different nanofluids and the increment in the Prandtl number for the same Re [51]. Furthermore, the hydrodynamic properties (ΔP and f) increase in the twisted pipe by 265.454% relative to the plain pipe using the same working fluids (DW and different nanofluids). SiO_2/DW presents the maximum augmentations in the hydrodynamic property values with 167.114% (plain pipe relative to DW) and 166.994% (twisted pipe relative to DW). Meanwhile, the lowest augmentations in the hydrodynamic property values are presented by SiO_2 + Al_2O_3 + ZnO/DW with 41.588% (plain pipe relative to DW) and 41.518% (twisted pipe relative to DW). Helical profiled pipe suffering of high-pressure loss because of the swirling flows and turbulent intensities due to the larger surface area, which enhanced the interaction of the pressure forces with inertial forces in the boundary layers. Meanwhile, the increased flow resistance created by the counter-collision of fluid streams is attributed to the more considerable friction losses [50]. This phenomenon may lead to the division of the cross-sectional area in the tube; thus, the flow velocity increases, and the complicated pipeline structure enhances the disturbance, which leads to the increase in the flow resistance [52].

Figure 7(a and b) depicts the local Nusselt number against axial position for plain and twisted-tape pipes filled with various nanofluids at 4vol% and Re = 9,000. The collected data, comprising the bulk and wall temperatures, as well as the heat flow of the test area, could be used to compute the local Nusselt number. The results clearly reveal insignificant variations in the Nusselt number data of the nanofluids in the plain pipe under the fully developed condition of the turbulent flow region and the local Nusselt number in the thermally developing region because the local Nusselt number is somewhat enhanced [53]. Meanwhile, because the axial locations are measured at the helical cross sections of twisted-tape pipe, Figure 7(b) displays more variations than Figure 7(a).

The double effects of thermal and frictional properties should be considered in engineering applications. The thermohydraulic efficiency ($\eta_{\text{Thermohydraulic}}$) was proposed to evaluate the total performance of plain and helical profiled pipes in more depth. The formula for calculating the ($\eta_{\text{Thermohydraulic}}$) value is presented in equation (22). Overall, $\eta_{\text{Thermohydraulic}} > 1$ for all tested working fluids (DW, single, hybrid, and ternary nanofluids) versus Reynolds numbers (Figure 8). When the Reynolds number is increased, the $\eta_{\text{Thermohydraulic}}$ rises quickly at first, then gradually declines. As a result, there is a crucial Reynolds number, and the largest value of $\eta_{\text{Thermohydraulic}}$ may be produced. The heat transfer augmentation effect supplied

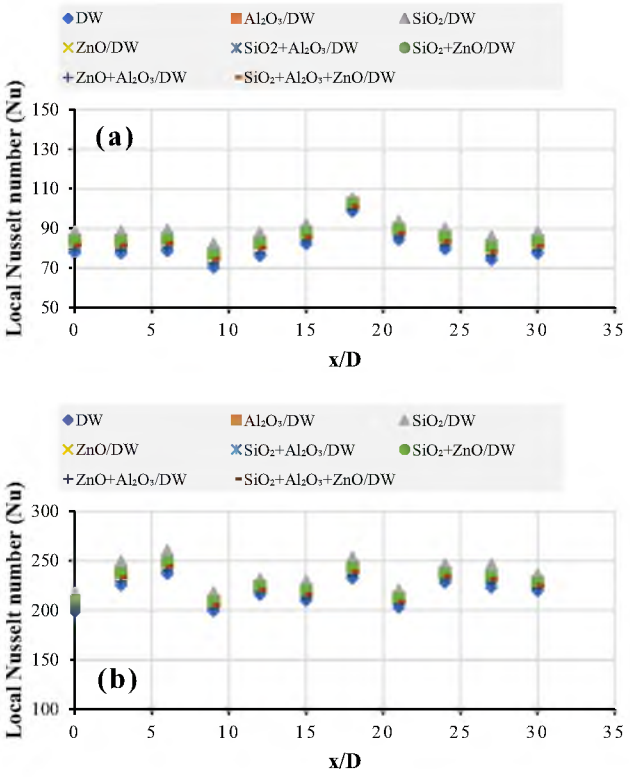

Figure 7: Comparison of the local Nusselt number and the non-dimensional axial distance (x/D) at Re = 9,000 and 4vol% of various nanofluid types: (a) plain pipe and (b) twisted tape pipe.

by the nanoparticle suspension is no longer noticeable at Reynolds numbers of 7,000 and 9,000 or greater than 15,000, and the impact of frictional pressure drop progressively rises, resulting in a decline in thermohydraulic efficiency values [52]. The negative effect of frictional pressure drop in the helical pipe on the $\eta_{\text{Thermohydraulic}}$ is the smallest. The heat exchanging effect caused by its disturbance is the maximum; therefore, the $\eta_{\text{Thermohydraulic}}$ value peaks at the moment. Different types of nanofluids show almost the

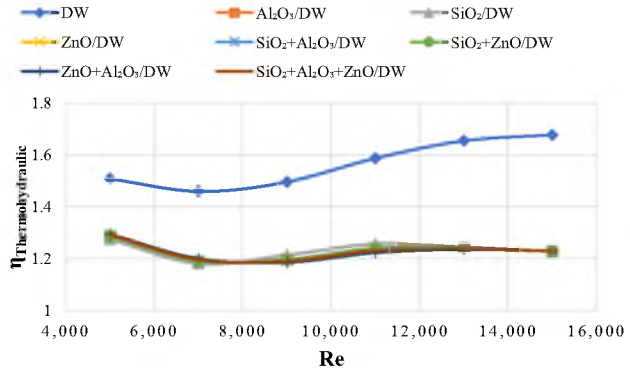

Figure 8: Thermohydraulic performance of plain and twisted pipes using DW, single, hybrid, and ternary nanofluids at 4vol%.

same thermohydraulic trends/behaviors. In general, the suspension of nanoparticles in DW shows the opposing effects as follows [54]:

1) increased thermal conductivity and nanoparticle collisions improve the heat transport rate,
2) the increase in working fluid viscosity reduces fluid flow and, therefore, the heat transfer rate decreases.

The current result indicates that improved thermal conductivity and increased nanoparticle collisions at the current range are more significant than the effect of increased viscosity. In this study, DW shows higher $\eta_{\text{Thermohydraulic}}$ values than nanofluids. DW achieves the highest $\eta_{\text{Thermohydraulic}}$ value at Re = 15,000 with 1.678. The lowest $\eta_{\text{Thermohydraulic}}$ value is achieved by SiO_2/DW at Re = 7,000 with 1.181.

4.6 Velocity contours and profiles

Figure A1 shows the velocity contours and profile of DW, single nanofluids (Al_2O_3/DW, SiO_2/DW, and ZnO/DW), hybrid nanofluids (SiO_2 + Al_2O_3/DW, SiO_2 + ZnO/DW, and ZnO + Al_2O_3/DW), and ternary nanofluids (SiO_2 + Al_2O_3 + ZnO/DW). Velocity contours of twisted pipe under different planes (slices), namely, P-1, P-2, P-13, P-14, and P-27 were presented at Re = 9,000. The five planes were chosen to represent various twisted-tape directions. Figure A1 indicates that the insertion of the twisted tape leads to the significant increase in the velocity of the flow near it. Moreover, figures illustrate that the velocity at the center of the tube near the twisted tape is larger, and consequently, the flow resistance increases. Clearly, because of the geometry of twisted tapes and the fluid having to overcome additional barriers to flow through the pipe, the ΔP of the twisted tape is greater than the smooth one.

5 Conclusions

Plain and tilted twisted-tape pipes were computationally evaluated *via* k-omega SST turbulence models in the $5{,}000 \leq \text{Re} \leq 15{,}000$. Single nanofluids ($Al_2O_3$/DW, SiO_2/DW, and ZnO/DW), hybrid nanofluids (SiO_2 + Al_2O_3/DW, SiO_2 + ZnO/DW, and ZnO + Al_2O_3/DW) in the mixture ratio of 80:20, and ternary nanofluids (SiO_2 + Al_2O_3 + ZnO/DW) in the mixture ratio of (60:20:20) were estimated in different volumetric concentrations (1, 2, 3, and 4%). Other thermohydraulic parameters were studied, and the most significant conclusions are as follows:

1) Thermophysical properties were estimated at 303 K. The higher increments in thermal density, thermal conductivity, and viscosity were 18.554% for 4vol%-ZnO/DW, 20.600% for 4vol%-Al_2O_3/DW, and 67.383% for 4vol%-Al_2O_3/DW, respectively. Meanwhile, the higher reduction in specific heat was presented by 4vol%-ZnO/DW with 14.514%.
2) The average errors among grids 1, 2, 3, and 4 with Dittus–Boelter and Blasius equations were 4.233 and 2.102%, 3.244 and 4.773%, 3.124 and 5.843%, and 2.947 and 6.683%, respectively.
3) SiO_2/DW recorded the lower outlet temperature at 4vol% and Re = 900 such as 310.933 K (plain pipe) and 313.842 K (twisted pipe).
4) ZnO/DW presented the highest increment of heat gain at 4vol% and Re = 900 with 39.259% (plain pipe) and 38.914% (twisted pipe) relative to DW.
5) Heat transfer parameters enhanced by about 86.978% when using SiO_2/DW at 4vol% and Re = 900 through twisted pipe relative to plain pipe.
6) SiO_2/DW presented the higher pressure drop at 4vol % and Re = 900 with 167.114% (plain pipe) and 166.994% (twisted pipe) relative to DW.
7) The plots of local Nusselt number versus the axial locations revealed insignificant variations in both plain and twisted-tape pipes using different types of working fluids.
8) All tested heat transfer fluids showed $\eta_{\text{Thermohydraulic}} > 1$. At Re = 900, DW recorded the best $\eta_{\text{Thermohydraulic}}$ with 1.496 followed by SiO_2/DW with 1.214. Meanwhile, the higher $\eta_{\text{Thermohydraulic}}$ value was 1.678 using water at Re = 15,000.

Funding information: This work was funded by Universiti Teknologi Malaysia (UTM), operated by Research Management Center (RMC), under the Research University Grant number (06E10).

Author contributions: Omer A. Alawi: conceptualization, formal analysis, writing – original draft; Haslinda Mohamed Kamar and Nadhir Al-Ansari: funding acquisition; Omer A. Alawi, Omar A. Hussein, Raad Z. Homod: investigation; Omer A. Alawi, Ali H. Abdelrazek, Waqar Ahmed: methodology; Haslinda Mohamed Kamar, Omer A. Alawi, Nadhir Al-Ansari: project administration; Haslinda Mohamed Kamar: supervision; Zaher Mundher Yaseen, Ali M. Ahmed, Mahmoud Eltaweel: writing – review and editing. All

authors have accepted responsibility for the entire content of this manuscript and approved its submission.

Conflict of interest: The authors state no conflict of interest.

References

[1] Alawi OA, Kamar HM, Hussein OA, Mallah AR, Mohammed HA, Khiadani M, et al. Effects of binary hybrid nanofluid on heat transfer and fluid flow in a triangular-corrugated channel: An experimental and numerical study. Powder Technol. 2022;395:267–79 doi: 10.1016/j.powtec.2021.09.046.

[2] Homod RZ, Togun H A, Ateeq A, Al-Mousawi F M, Yaseen Z, Al-Kouz W, et al. An innovative clustering technique to generate hybrid modeling of cooling coils for energy analysis: A case study for control performance in HVAC systems. SSRN Electron J. 2022;166:112676. doi: 10.2139/ssrn.4037290

[3] Saadah A, Abdullah S, Sopian K. The effect of linearly increasing/decreasing pitch ratio twisted tape with various progression rate and nanofluid towards the system performance. Therm Sci Eng Prog. 2021;25:100979.

[4] Zhang J, Zhu X, Mondejar ME, Haglind F. A review of heat transfer enhancement techniques in plate heat exchangers. Renewable Sustainable Energy Rev. 2019;101:305–28.

[5] Awais M, Ullah N, Ahmad J, Sikandar F, Ehsan MM, Salehin S, et al. Heat transfer and pressure drop performance of nanofluid: A state-of-the-art review. Int J Thermofluids. 2021;9:100065.

[6] Ajeel RK, Salim WSI, Sopian K, Yusoff MZ, Hasnan K, Ibrahim A, et al. Turbulent convective heat transfer of silica oxide nanofluid through corrugated channels: An experimental and numerical study. Int J Heat Mass Transf. 2019;145:118806. doi: 10.1016/j.ijheatmasstransfer.2019.118806

[7] Vallejo JP, Prado JI, Lugo L. Hybrid or mono nanofluids for convective heat transfer applications. A critical review of experimental research. Appl Therm Eng. 2021;203:117926.

[8] Tao H, Alawi OA, Hussein OA, Ahmed W, Abdelrazek AH, Homod RZ, et al. Thermohydraulic analysis of covalent and noncovalent functionalized graphene nanoplatelets in circular tube fitted with turbulators. Sci Rep. 2022;12:1–24. doi: 10.1038/s41598-022-22315-9

[9] Singh SK, Sarkar J. Hydrothermal performance comparison of modified twisted tapes and wire coils in tubular heat exchanger using hybrid nanofluid. Int J Therm Sci. 2021;166:106990.

[10] Khoshvaght-Aliabadi M, Davoudi S, Dibaei MH. Performance of agitated-vessel U tube heat exchanger using spiky twisted tapes and water based metallic nanofluids. Chem Eng Res Des. 2018;133:26–39.

[11] Akyürek EF, Geliş K, Şahin B, Manay E. Experimental analysis for heat transfer of nanofluid with wire coil turbulators in a concentric tube heat exchanger. Results Phys. 2018;9:376–89.

[12] Eiamsa-ard S, Wongcharee K, Kunnarak K, Kumar M, Chuwattabakul V. Heat transfer enhancement of TiO2-water nanofluid flow in dimpled tube with twisted tape insert. Heat Mass Transf. 2019;55:2987–3001.

[13] He W, Toghraie D, Lotfipour A, Pourfattah F, Karimipour A, Afrand M. Effect of twisted-tape inserts and nanofluid on flow field and heat transfer characteristics in a tube. Int Commun Heat Mass Transf. 2020;110:104440.

[14] Bazdidi-Tehrani F, Khanmohamadi SM, Vasefi SI. Evaluation of turbulent forced convection of non-Newtonian aqueous solution of CMC/CuO nanofluid in a tube with twisted tape inserts. Adv Powder Technol. 2020;31:1100–13.

[15] Miandoab AR, Bagherzadeh SA, Isfahani AHM. Numerical study of the effects of twisted-tape inserts on heat transfer parameters and pressure drop across a tube carrying graphene oxide nanofluid: An optimization by implementation of artificial neural network and genetic algorithm. Eng Anal Bound Elem. 2022;140:1–11.

[16] Singh SK, Sarkar J. Improving hydrothermal performance of double-tube heat exchanger with modified twisted tape inserts using hybrid nanofluid. J Therm Anal Calorim. 2021;143:4287–98.

[17] Maddah H, Aghayari R, Mirzaee M, Ahmadi MH, Sadeghzadeh M, Chamkha AJ. Factorial experimental design for the thermal performance of a double pipe heat exchanger using Al2O3–TiO2 hybrid nanofluid. Int Commun Heat Mass Transf. 2018;97:92–102.

[18] Singh SK, Sarkar J. Experimental hydrothermal characteristics of concentric tube heat exchanger with V-cut twisted tape turbulator using PCM dispersed mono/hybrid nanofluids. Exp Heat Transf. 2020;34:1–22.

[19] Bahiraei M, Mazaheri N, Aliee F. Second law analysis of a hybrid nanofluid in tubes equipped with double twisted tape inserts. Powder Technol. 2019;345:692–703.

[20] Singh SK, Sarkar J. Improving hydrothermal performance of hybrid nanofluid in double tube heat exchanger using tapered wire coil turbulator. Adv Powder Technol. 2020;31:2092–100.

[21] Sani FH, Pourfallah M, Gholinia M. The effect of MoS2–Ag/H2O hybrid nanofluid on improving the performance of a solar collector by placing wavy strips in the absorber tube. Case Stud Therm Eng. 2022;30:101760.

[22] Almitani KH, Alzaed A, Alahmadi A, Sharifpur M, Momin M. The influence of the geometric shape of the symmetrical twisted turbulator on the performance of parabolic solar collector having hybrid nanofluid: Numerical approach using two-phase model. Sustainable Energy Technol Assess. 2022;51:101882.

[23] Suliman M, Ibrahim M, Saeed T. Improvement of efficiency and PEC of parabolic solar collector containing EG–Cu–SWCNT hybrid nanofluid using internal helical fins. Sustainable Energy Technol Assess. 2022;52:102111.

[24] Kashyap S, Sarkar J, Kumar A. Performance enhancement of regenerative evaporative cooler by surface alterations and using ternary hybrid nanofluids. Energy. 2021;225:120199.

[25] Sahu M, Sarkar J, Chandra L. Steady-state and transient hydrothermal analyses of single-phase natural circulation loop using water-based tri-hybrid nanofluids. AIChE J. 2021;67:e17179.

[26] Alawi OA, Kamar HM, Mallah AR, Mohammed HA, Sabrudin MAS, Newaz KMS, et al. Experimental and theoretical analysis of energy efficiency in a flat plate solar collector using

monolayer graphene nanofluids. Sustainability. 2021;13(10):5416. doi: 10.3390/su13105416
[27] Mohammad RS, Aldlemy MS, Al Hassan MS, Abdulla AI, Scholz M, Yaseen ZM. Frictional pressure drop and cost savings for graphene nanoplatelets nanofluids in turbulent flow environments. Nanomaterials. 2021;11:1–17.
[28] Aldlemy M, Ahammed SJ, Obando ED, Bayatvarkeshi M. Numerical simulation on the effect of pipe roughness in turbulent flow. Knowl Eng Sci. 2022;3:37–44.
[29] Cabello R, Popescu AEP, Bonet-Ruiz J, Cantarell DC, Llorens J. Heat transfer in pipes with twisted tapes: CFD simulations and validation. Comput Chem Eng. 2022;166:107971.
[30] Xuan Y, Roetzel W. Conceptions for heat transfer correlation of nanofluids. Int J Heat Mass Transf. 2000;43:3701–7. doi: 10.1016/S0017-9310(99)00369-5
[31] Abdelrazek AH, Kazi SN, Alawi OA, Yusoff N, Oon CS, Ali HM. Heat transfer and pressure drop investigation through pipe with different shapes using different types of nanofluids. J Therm Anal Calorim. 2020;139:1637–53. doi: 10.1007/s10973-019-08562-5
[32] Sadri R, Mallah AR, Hosseini M, Ahmadi G, Kazi SN, Dabbagh A, et al. CFD modeling of turbulent convection heat transfer of nanofluids containing green functionalized graphene nanoplatelets flowing in a horizontal tube: Comparison with experimental data. J Mol Liq. 2018;269:152–9.
[33] Menter FR. Two-equation eddy-viscosity turbulence models for engineering applications. AIAA J. 1994;32:1598–605.
[34] Bashtani I, Esfahani JA, Kim KC. Effects of water-aluminum oxide nanofluid on double pipe heat exchanger with gear disc turbulators: A numerical investigation. J Taiwan Inst Chem Eng. 2021;124:63–74.
[35] Bahiraei M, Mazaheri N, Aliee F, Safaei MR. Thermo-hydraulic performance of a biological nanofluid containing graphene nanoplatelets within a tube enhanced with rotating twisted tape. Powder Technol. 2019;355:278–88. doi: 10.1016/j.powtec.2019.07.053
[36] Le Ba T, Mahian O, Wongwises S, Szilágyi IM. Review on the recent progress in the preparation and stability of graphene-based nanofluids. J Therm Anal Calorim. 2020;142:1145–72.
[37] Adun H, Kavaz D, Dagbasi M. Review of ternary hybrid nanofluid: Synthesis, stability, thermophysical properties, heat transfer applications, and environmental effects. J Clean Prod. 2021;328:129525.
[38] Giwa SO, Sharifpur M, Ahmadi MH, Sohel Murshed SM, Meyer JP. Experimental investigation on stability, viscosity, and electrical conductivity of water-based hybrid nanofluid of MWCNT-Fe2O3. Nanomaterials. 2021;11:136.
[39] Venkateswarlu B, Satya Narayana PV. Cu-Al2O3/H2O hybrid nanofluid flow past a porous stretching sheet due to temperature-dependent viscosity and viscous dissipation. Heat Transf. 2021;50:432–9.
[40] Rostami S, Toghraie D, Shabani B, Sina N, Barnoon P. Measurement of the thermal conductivity of MWCNT-CuO/water hybrid nanofluid using artificial neural networks (ANNs). J Therm Anal Calorim. 2021;143:1097–5.
[41] Xuan Z, Zhai Y, Ma M, Li Y, Wang H. Thermo-economic performance and sensitivity analysis of ternary hybrid nanofluids. J Mol Liq. 2021;323:114889.
[42] Ahmed W, Kazi SN, Chowdhury ZZ, Johan MRB, Soudagar MEM, Mujtaba MA, et al. Ultrasonic assisted new Al2O3@ TiO2-ZnO/DW ternary composites nanofluids for enhanced energy transportation in a closed horizontal circular flow passage. Int Commun Heat Mass Transf. 2021;120:105018.
[43] Sahoo RR. Thermo-hydraulic characteristics of radiator with various shape nanoparticle-based ternary hybrid nanofluid. Powder Technol. 2020;370:19–28.
[44] Alawi OA, Sidik NAC, Xian HW, Kean TH, Kazi SN. Thermal conductivity and viscosity models of metallic oxides nanofluids. Int J Heat Mass Transf. 2018;116:1314–25. doi: 10.1016/j.ijheatmasstransfer.2017.09.133
[45] Eiamsa-ard S, Thianpong C, Eiamsa-ard P. Turbulent heat transfer enhancement by counter/co-swirling flow in a tube fitted with twin twisted tapes. Exp Therm Fluid Sci. 2010;34:53–62.
[46] Hamzah MH, Sidik NAC, Ken TL, Mamat R, Najafi G. Factors affecting the performance of hybrid nanofluids: a comprehensive review. Int J Heat Mass Transf. 2017;115:630–46.
[47] Sahoo RR, Kumar V. Development of a new correlation to determine the viscosity of ternary hybrid nanofluid. Int Commun Heat Mass Transf. 2020;111:104451.
[48] Mousavi SM, Esmaeilzadeh F, Wang XP. Effects of temperature and particles volume concentration on the thermophysical properties and the rheological behavior of CuO/MgO/TiO2 aqueous ternary hybrid nanofluid. J Therm Anal Calorim. 2019;137:879–901.
[49] Alnaqi AA, Alsarraf J, Al-Rashed AAAA. Hydrothermal effects of using two twisted tape inserts in a parabolic trough solar collector filled with MgO-MWCNT/thermal oil hybrid nanofluid. Sustainable Energy Technol Assess. 2021;47:101331.
[50] Thianpong C, Wongcharee K, Safikhani H, Chokphoemphun S, Saysroy A, Skullong S, et al. Multi objective optimization of TiO2/water nanofluid flow within a heat exchanger enhanced with loose-fit delta-wing twisted tape inserts. Int J Therm Sci. 2022;172:107318.
[51] Dagdevir T, Ozceyhan V. An experimental study on heat transfer enhancement and flow characteristics of a tube with plain, perforated and dimpled twisted tape inserts. Int J Therm Sci. 2021;159:106564.
[52] Wang Y, Qi C, Ding Z, Tu J, Zhao R. Numerical simulation of flow and heat transfer characteristics of nanofluids in built-in porous twisted tape tube. Powder Technol. 2021;392:570–86.
[53] Beiki H. Developing convective mass transfer of nanofluids in fully developed flow regimes in a circular tube: modeling using fuzzy inference system and ANFIS. Int J Heat Mass Transf. 2021;173:121285.
[54] Wongcharee K, Eiamsa-ard S. Heat transfer enhancement by using CuO/water nanofluid in corrugated tube equipped with twisted tape. Int Commun Heat Mass Transf. 2012;39:251–7.

Appendix

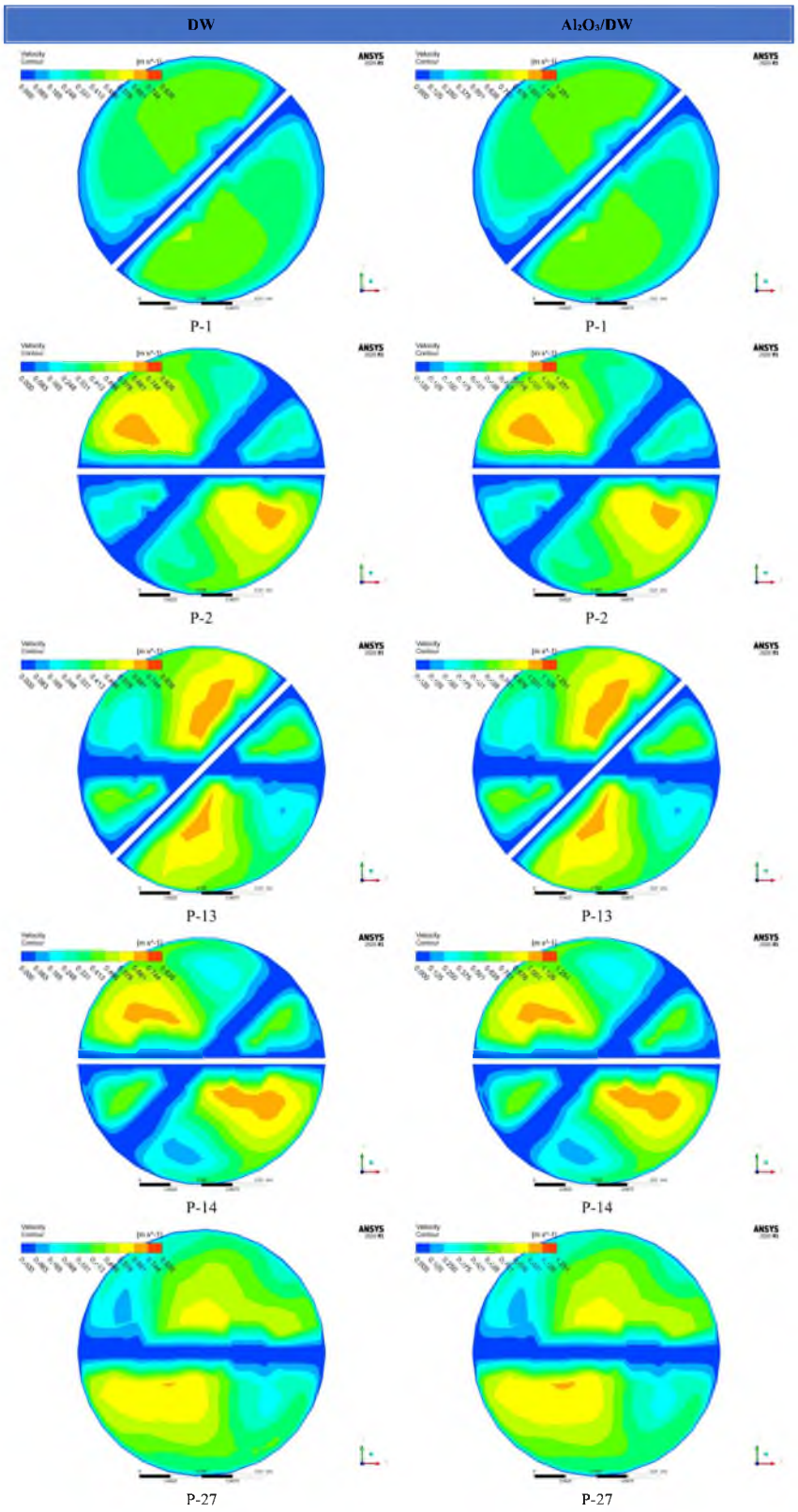

Figure A1: Velocity profiles of DW, single, hybrid, and triple nanofluids under different planes at Re = 9,000.

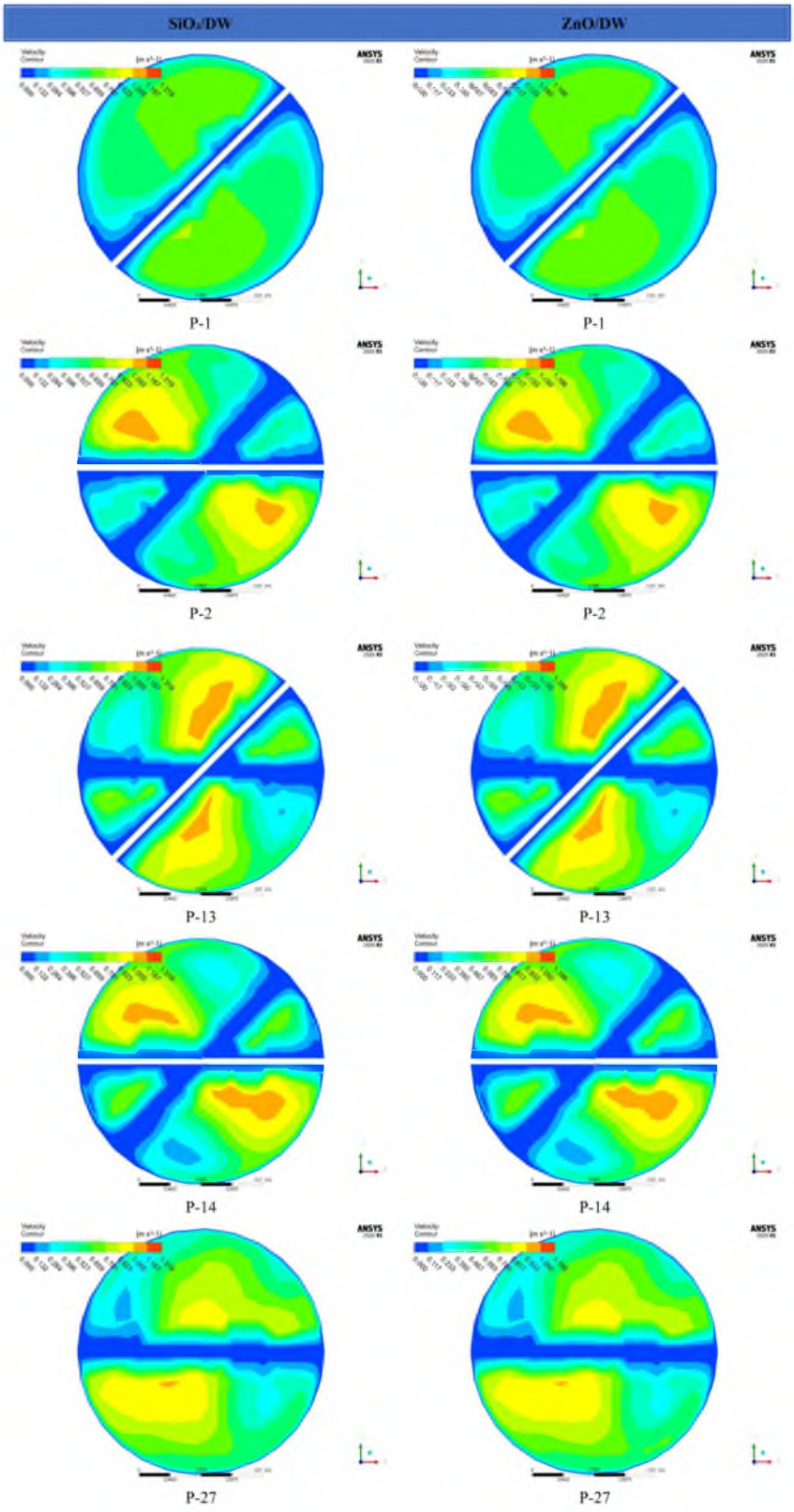

Figure A1: (*Continued*)

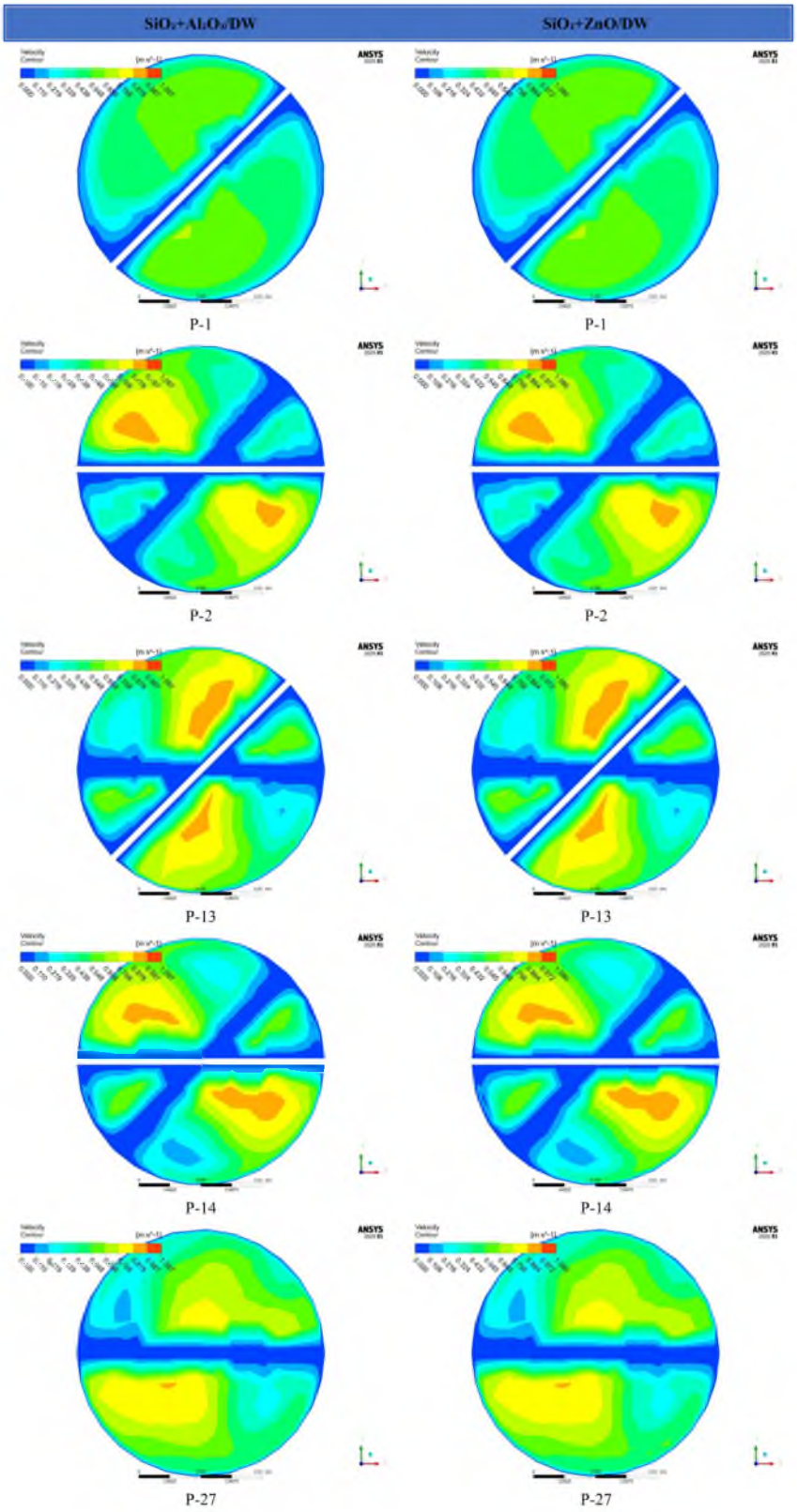

Figure A1: (*Continued*)

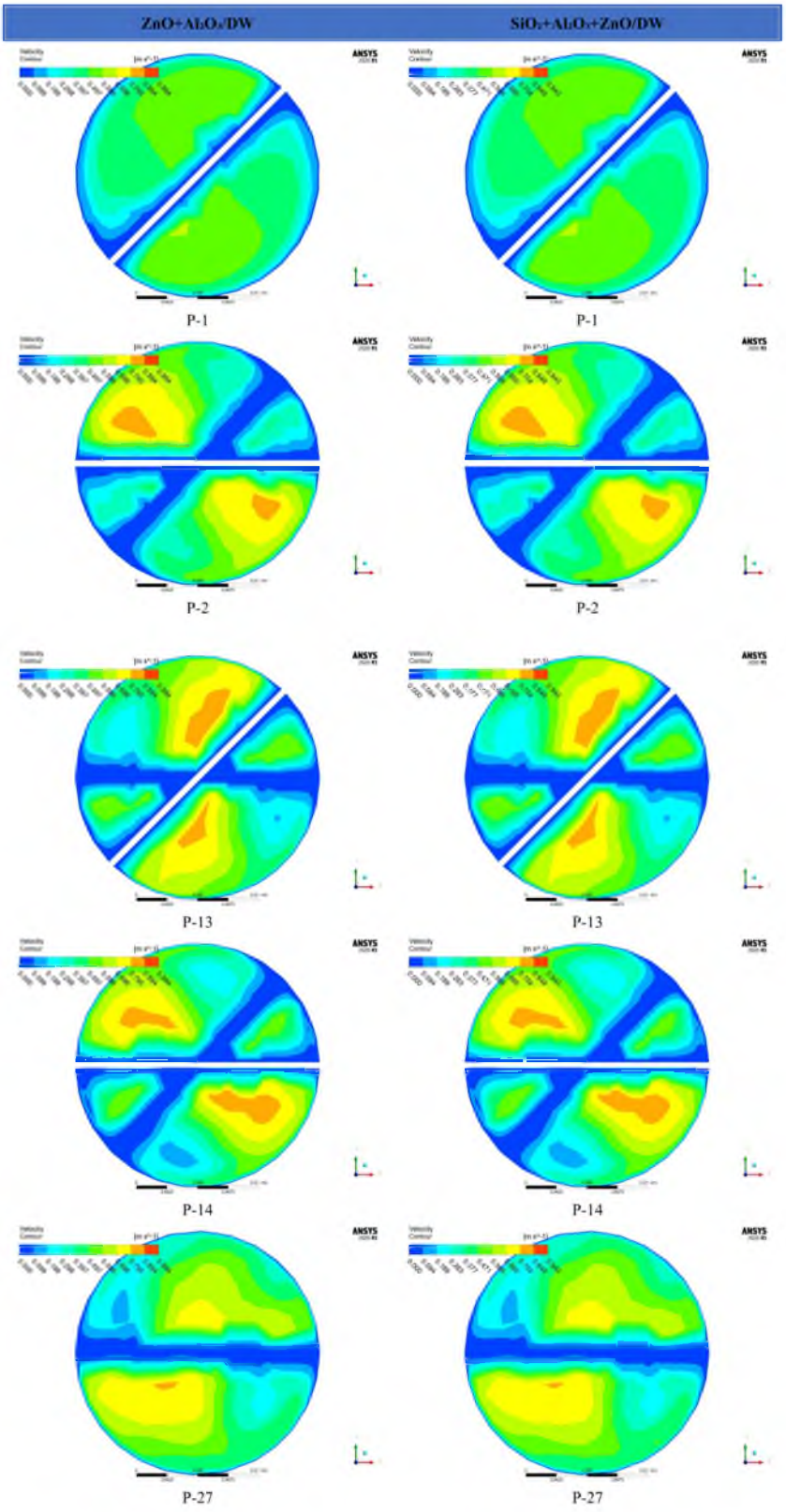

Figure A1: (*Continued*)